Probabilistic stimulation mapping from intra-operative thalamic deep brain stimulation data in essential tremor

Dorian Vogel, Teresa Nordin, Stefanie Feiler, Karin Wardell, Jérôme Coste, Jean-Jacques Lemaire, Simone Hemm-Ode

Journal of Neural Engineering

Probabilistic stimulation mapping from intra-operative thalamic deep brain stimulation data in essential tremor

To cite this article before publication: Dorian Vogel *et al* 2024 *J. Neural Eng.* in press https://doi.org/10.1088/1741-2552/ad4742

Probabilistic Stimulation Mapping from Intra-Operative Thalamic Deep Brain Stimulation Data in Essential Tremor.

Dorian VOGEL[a], Teresa NORDIN[c], Stefanie FEILER[b], Karin WÅRDELL[a,c], Jérôme COSTE[d,e], Jean-Jacques LEMAIRE[d,e], Simone HEMM[a,c]

[a]Institute for Medical Engineering and Medical Informatics, School of Life Sciences, University of Applied Sciences and Arts Northwestern Switzerland, Hofackerstrasse 30, Muttenz, Switzerland

[b]Dynamics and statistics of complex systems, School of Life Sciences, University of Applied Sciences and Arts Northwestern Switzerland, Hofackerstrasse 30, Muttenz, Switzerland

[c]Department of Biomedical Engineering, Linköping University, Campus US, Linköping, Sweden

[d]Université Clermont Auvergne, CNRS, SIGMA Clermont, Institut Pascal, Clermont-Ferrand, France

[e]Service de Neurochirurgie, Hôpital Gabriel-Montpied, Centre Hospitalier Universitaire de Clermont-Ferrand, 58 rue Montalembert, Clermont-Ferrand, France

Corresponding author:

Dorian Vogel

Institute for Medical Engineering and Medical Informatics

School of Life Sciences

University of Applied Sciences and Arts Northwestern Switzerland

Hofackerstrasse 30

4132 Muttenz, Switzerland

email: dorian.vogel@fhnw.ch

Keywords:

Deep Brain Stimulation (DBS), Probabilistic Stimulation Map, Atlas, Essential Tremor, Intra-Operative Stimulation, Vim, Quantitative Symptoms Assessment.

Abbreviations

CGM: Corpus geniculatum Medial, CT: Computed Tomography, DL: Dorsolateral Thalamus, DM: Dorsomedial Thalamus, DRTT: Denta-Rubo Thalamic Tract, EF: electric field, ET: essential tremor, ETRS: Essential Tremor Rating Scale, FF: fields of Forel, FEM: finite element method, GPi: Globus Pallidus Internus, InL: intermediolateral thalamus, LaPf: Parafascicular Thalamus, LMM: Linear Mixed Model, Med: Medial Thalmus, MER: micro-electrode recording, MNI: Montreal Neurological Institute, MR: Magnetic resonance, MRI: Magnetic Resonance Imaging, PD: Parkinson's disease, PPn: Peripeduncular Nucleus, PSA: posterior subthalamic area, PSM: probabilistic stimulation map, Pu: Pulvinar Thalamus, SN: Substancia Nigra, STN: subthalamic nucleus, UPDRS: Universal Parkinson's Disease Rating Scale, VCL: ventrocaudal-lateral thalamus, VO: ventro-oral thalamus, VCM: ventrocaudal-medial thalamus, Vc: ventrocaudal thalamus (VCM+VCL), Vim: ventral intermediate nucleus of the thalamus, VTA: volume of tissue activated, WAIR: white-matter attenuated inversion recovery, Zi: Zona incerta

Abstract

Deep brain stimulation (DBS) is a therapy for Parkinson's disease (PD) and essential tremor (ET). The mechanism of action of DBS is still incompletely understood. Retrospective group analysis of intra-operative data recorded from ET patients implanted in the ventral intermediate nucleus of the thalamus (Vim) is rare. Intra-operative stimulation tests generate rich data and their use in group analysis has not yet been explored.

Objective: To implement, evaluate, and apply a group analysis workflow to generate probabilistic stimulation maps (PSM) using intra-operative stimulation data from ET patients implanted in Vim.

A group-specific anatomical template was constructed based on the Magnetic Resonance Imaging (MRI) scans of 6 ET patients and 13 PD patients. Intra-operative test data (total: n=1821) from the 6 ET patients was analyzed: patient-specific electric field simulations together with tremor assessments obtained by a wrist-based acceleration sensor were transferred to this template. Occurrence and weighted mean maps were generated. Voxels associated with symptomatic response were identified through a linear mixed model approach to form a PSM. Improvements predicted by the PSM were compared to those clinically assessed. Finally, the PSM clusters were compared to those obtained in a multicenter study using data from chronic stimulation effects in ET.

Regions responsible for improvement identified on the PSM were in the posterior sub-thalamic area (PSA) and at the border between the Vim and ventro-oral nucleus of the thalamus (VO). The comparison with literature revealed a center-to-center distance of less than 5mm and an overlap score (Dice) of 0.4 between the significant clusters.

Our workflow and intra-operative test data from 6 ET-Vim patients identified effective stimulation areas in PSA and around Vim and VO, affirming existing medical literature. This study supports the potential of probabilistic analysis of intra-operative stimulation test data to reveal DBS's action mechanisms and to assist surgical planning.

1. Background

Deep brain stimulation (DBS) is a well-established therapy for patients with movement disorders such as Parkinson's disease (PD) (Benabid *et al.*, 1994; Hariz, 2017) or essential tremor (ET) (Benabid *et al.*, 1993). Electrical stimulation is delivered to the structures in the center of the brain with electrodes implanted surgically. A crucial parameter for the therapy is the location of electrode contacts in relation to the deep brain structures. To pinpoint the optimal placement of the electrode, but also because the exact mechanisms of action are not fully understood, stimulation tests are still common practice during surgery. These may be conducted using the DBS lead or so-called exploration electrodes when micro-electrode recording (MER) is used for target refinement.

To investigate the mechanisms of action of DBS, normative analysis of data collected during chronic stimulation in patients has become an intense topic in research (Lozano *et al.*, 2019; Elias *et al.*, 2021; Roquemaurel *et al.*, 2021). The general approach consists of transforming the magnetic resonance (MR) images from several patients of a cohort into a common reference space where the stimulation data can be analyzed. Since most studies focus on post-operative screening where the

electrode is already implanted, the anatomical region and setting combinations explored in each patient is limited. To compensate, larger numbers of patients are required, which introduces other problems such as increasing the processing time of the anatomical normalization or the difficulty in obtaining homogeneous, high-quality datasets. As a result, those studies often rely on sources of data external to the cohort. These include anatomical reference spaces from the Montreal Neurological Institute (MNI) (Fonov *et al.*, 2009), outlines of anatomical structures such as Schaltenbrand and Wahren (Schaltenbrand, 1977), Morel's (Morel, 2007) or the YeB atlas (Yelnik *et al.*, 2007). Sometimes connectivity information is gathered from the patients themselves (Akram *et al.*, 2018) or derived from the Human Connectome Project (Horn and Blankenburg, 2016). To avoid mixing anatomical information external to a cohort, we previously published the creation of group-specific templates including outlines of deep brain structures by a single expert (Vogel *et al.*, 2020, 2021).

The anatomical location of stimulation can be approximated to the coordinates of the center of the active contact (Nowinski *et al.*, 2005; Lalys *et al.*, 2013; Barbe *et al.*, 2018) or to a sphere (Eisenstein *et al.*, 2014; Dembek *et al.*, 2017). Several groups have presented the use of finite element model (FEM) simulation to estimate the extent of stimulation (Butson *et al.*, 2007; Aström *et al.*, 2009; Howell and McIntyre, 2017; Butenko *et al.*, 2020). Conductivity models for those can be of varying levels of complexity, from homogeneous gray matter to patient-specific, isotropic or anisotropic tissue properties (Åström, Lemaire and Wårdell, 2012; Nordin *et al.*, 2019). To analyze the spread of the stimulation within brain tissue and the therapeutic effect of the stimulation, many studies use clinical scores estimated at different steps before and after the surgery such as the universal parkinson's disease rating scale (UPDRS) score for PD patients (Dembek *et al.*, 2019; Horn *et al.*, 2019; Elias *et al.*, 2021), the essential tremor rating scale (ETRS) for ET patients (Åström *et al.*, 2018) or a percentage-based assessment of tremor reduction (Dembek *et al.*, 2017). However, these metrics are subject to intra- and inter-rater variability. To reach a more objective and reproducible evaluation of the symptoms, our group previously presented a method for quantitative assessment of tremor using a wrist-worn acceleration sensor (Shah *et al.*, 2017). Electric field (EF) simulations and quantitative tremor assessment were combined to create patient-specific stimulation maps (Shah *et al.*, 2020). The next step is to move to normative analysis: group-level template, simulation of the effect of intra-operative stimulation and quantitative assessment of the symptoms together have the potential to improve the understanding of DBS.

The aim of this study was to design and implement a custom probabilistic mapping workflow using intra-operative stimulation data for the creation of a probabilistic stimulation map (PSM). The approach is exemplified with stimulation data from a group of 6 ET patients implanted in the ventral intermediate nucleus of the thalamus (Vim).

2. Material and Methods

2.1. Clinical data

2.1.1. Patients

The study includes 19 patients (age: 50-84) who underwent bilateral DBS implantation (left hemisphere first) at the Department of Neurosurgery of the University Hospital in Clermont-Ferrand (France). Informed written consent was obtained from all patients (#2011-A00774-34/AU905). Of those patients, 13 were affected by PD and 6 by ET. Eleven of the PD patients were implanted in the subthalamic nucleus (STN) while the two remaining as well as all ET patients were implanted in the Vim. Structural MR images from all 19 patients were used for the creation of a group-specific anatomical template and the stimulation data from the six ET patients was used for the creation of a probabilistic stimulation map (Figure 1).

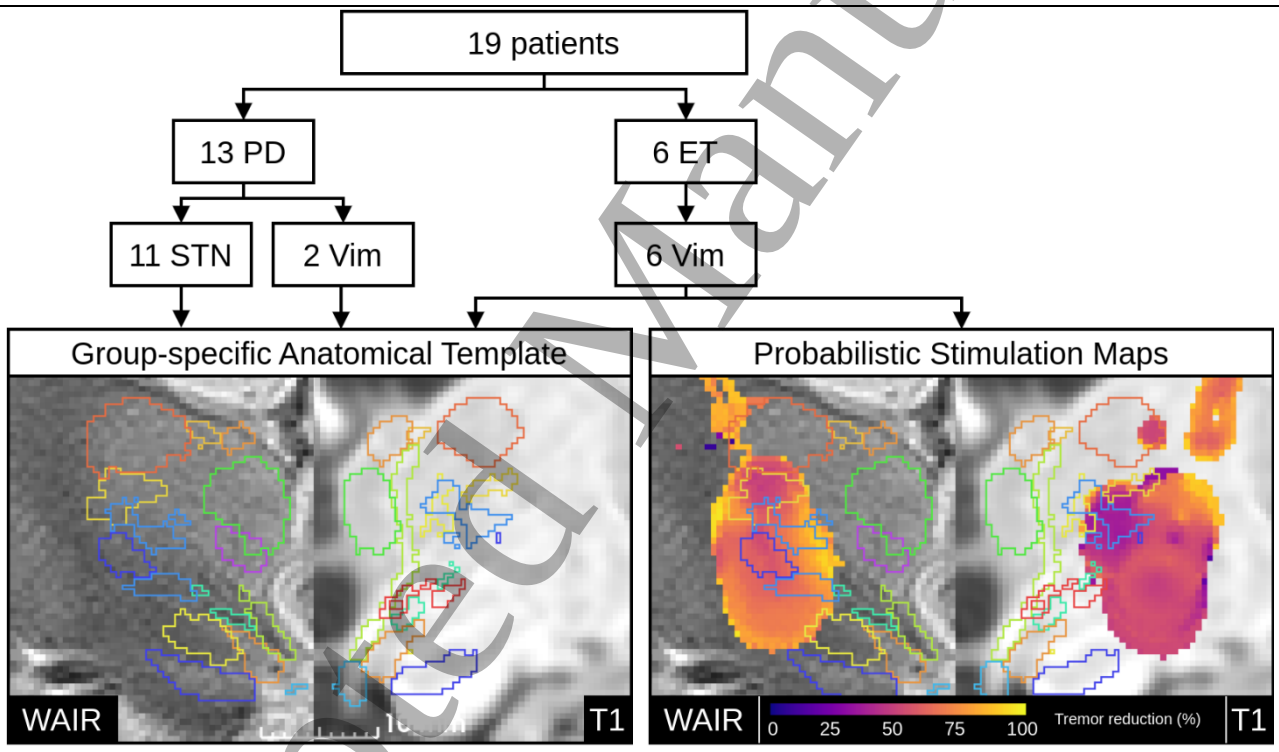

Figure 1: Composition of the cohort. The MRI datasets and outlines of the anatomical structures of all 19 patients were used for the creation of a group-specific anatomical template (left picture). Only the stimulation settings from essential tremor patients implanted in Vim were used for the creation of the probabilistic stimulation maps (right picture). Diseases: Parkinson's Disease (PD), Essential Tremor (ET), Targets: Subthalamic nucleus (STN), ventral intermediate nucleus of the thalamus (Vim). Background MRI modalities: T1, white matter attenuated inversion recovery (WAIR).

2.1.2. Imaging and surgical protocol

The procedure in this neurosurgery clinic takes place over two days (Vassal *et al.*, 2012). The first day is dedicated to imaging and planning. Pre-operative stereotactic T1-weighted (0.63mm x 0.63mm x 1.30mm) and WAIR (white matter inversion recovery) MRI (0.53mm x 0.53mm x 2.00mm)

(Magnotta *et al.*, 2000; Lemaire *et al.*, 2010) (Sonata, 1.5T, Siemens, Germany) are acquired. During trajectory planning, between 26 and 37 deep brain structures are labeled by the neurosurgeon for each patient using a 7T image set as anatomical reference (Lemaire *et al.*, 2010, 2019; Lemaire, 2021). The implantation itself takes place on the second day under local anesthesia after the acquisition of pre-operative computed tomography (CT) (0.59 mm x 0.59 mm x 1.25 mm). MER (Alpha-Omega Engineering, Israel) and symptom assessment during test stimulation are used. Test stimulation is done in the vicinity of the target (up to 8 mm before and 4 mm after in steps of 1 mm) with amplitudes up to 3 mA in steps of 0.2 mA using two parallel electrodes. The depth of implantation of the electrode is then selected to maximize the width of the therapeutic window i.e., respectively minimize and maximize the amplitude causing beneficial and adverse effects. Parallel to the stimulation tests, tremor was assessed for the six ET patients using an acceleration sensor worn by the patient on the wrist contralateral to the implanted side during routine tremor evaluation by the neurologist (arm hold, nose touch, finger tap) as described in (Shah *et al.*, 2017).

2.2. Patient-specific electric field simulation

The EF modeling method developed by Åström et al. (Åström *et al.*, 2009, 2015) which is freely available as the ELMA and DBSim apps (liu.se/en/article/ne-downloads) was applied to the six ET patients to simulate the distribution of the EF generated around the contact of each MER lead. The process is summarized in Figure 2.

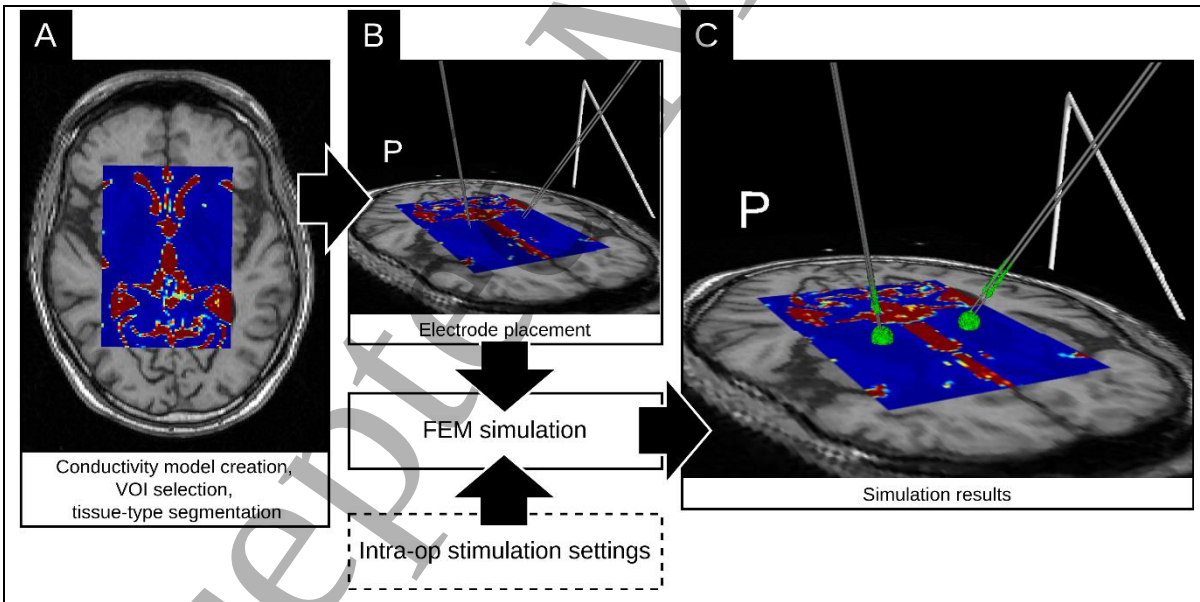

Figure 2: Electric field simulations. A brain conductivity model is first created based on segmentation from T1 MRI (A). The electrodes are placed along the planned trajectory using the Leksell arc settings (B). The intra-operative stimulation settings, conductivity, and lead models are used in the FEM simulations to estimate the electric field distribution (C).

First, a patient-specific, heterogeneous, isotropic tissue conductivity model (Figure 2A) was created for each patient using the Matlab-based ELMA software (Wårdell, Diczfalusy and Åström, 2011; Johansson, Alonso and Wårdell, 2019). Conductivity values in the model were assigned based on

the segmentation of gray matter, white matter, and cerebrospinal fluid on the T1-weighted images and the stimulation settings (amplitude, frequency, and pulse-width) tested during surgery (Gabriel, Lau and Gabriel, 1996; Wårdell *et al.*, 2013).

Second, an affine transform describing the placement of the electrode during the implantation in the patient reference space was built using Stereotaxia (Beninca *et al.*, 2017; Vogel, 2021), a plugin to 3DSlicer (Fedorov *et al.*, 2012). The process uses automatic detection and alignment of the Stereotactic fiducials to convert the Leksell arc settings used during the surgery (Figure 2, B) to image coordinates in the pre-operative T1.

Third, Comsol Multiphysics 5.5 (COMSOL AB, Sweden) was used as simulation environment with the volume of scalar conductivities to define the conductivity inside the simulation domain. The affine transformations were used to place the 3D model of the MER electrodes at the target position and a second affine transformation was applied to modulate the depth of the electrodes along the trajectory. The contact from the active MER electrodes was set as current source and the others were set to floating. The surface of the guide tubes used for the insertion of the test electrodes was used as ground connection. Using the Livelink for Matlab add-on for Comsol Multiphysics, the simulation model (Figure 2, C) was parametrized for each patient, hemisphere, number and depth of parallel electrodes and amplitudes used for the stimulation. A total of 1821 simulation results (Left: 959, Right:862) were saved as full FEM mesh files. A detailed summary of the number of tests per side and patient is provided in Table 1.

Table 1: Summary of the intra-operative stimulation tests conducted.

Side	Patient	Parallel MER Trajectories	Number of tests	Number of positions	Position Range (mm) [min - max]	Stimulation Amplitude (mA) [n; min - max]	Tremor Improvement (%)[mean(std)]
Left	000	central & posterior	276	8	-4 -> 3	25; 0.2 -> 5.0	59.3 (26.44)
	001	central & posterior	63	6	-5 -> 0	16; 0.2 -> 3.2	63.21 (34.39)
	002	central & posterior	62	5	-5 -> -1	16; 0.2 -> 3.0	52.36 (27.62)
	003	central & posterior	197	8	-5 -> 2	17; 0.2 -> 3.4	46.55 (25.12)
	004	central & posterior	168	9	-4 -> 4	15; 0.2 -> 3.0	48.44 (19.26)
	005	central & posterior	193	8	-3 -> 4	15; 0.2 -> 3.0	64.64 (27.32)
Right	000	central & posterior	176	8	-4 -> 3	25; 0.2 -> 5.0	40.18 (29.96)
	001	central & posterior	104	7	-5 -> 1	17; 0.2 -> 3.4	64.16 (27.17)
	002	central & posterior	113	6	-3 -> 2	15; 0.2 -> 3.0	48.39 (18.13)
	003	central & posterior	181	7	-5 -> 1	15; 0.2 -> 3.0	72.93 (25.49)
	004	central & posterior	104	5	-4 -> 0	15; 0.2 -> 3.0	64.98 (23.45)
	005	central & posterior	184	8	-3 -> 4	15; 0.2 -> 3.0	70.63 (22.63)

2.3. Anatomical Normalization

2.3.1. MRI images

To analyze the data in a common reference space, the anatomical normalization method previously published and optimized to produce full-brain images was employed (Vogel *et al.*, 2020, 2021). The anatomical normalization included the images from both PD and ET patients (N=19) in a process specially tailored to the image modalities available, using both T1 and WAIR MRI. It consists of an iterative registration of both modalities for each patient to a template that is updated after each iteration. The first reference was created using an affine transformation of the T1 images to the MNI152 (ICBM2009b) template (Fonov *et al.*, 2009). This was followed by six iterations of non-linear registrations using the coarse registration settings from (Ewert *et al.*, 2019). Four more iterations were run with finer registration settings (Vogel *et al.*, 2021). All non-linear registrations were run with ANTS-SyN (Avants *et al.*, 2010).

2.3.2. Labels of deep brain structures

The resulting affine transformations and deformation fields were used to transfer the outlines of structures of the thalamic and subthalamic region segmented during the planning and to obtain probabilistic definitions of 58 anatomical structures. These probabilistic definitions were converted to binary outlines for simplified visualization and analysis. This was done for each structure using region growing starting from the highest probability voxel. Growth was stopped when the volume of the structure in template space reached the average volume of the same structure in the original patient data.

2.4. Stimulation mapping

2.4.1. Simulation results post-processing.

Analogous to the outlines of anatomical structures, the results of EF simulations around the MER lead for all patients were transformed to template space. This was done by directly applying the appropriate transformations to the coordinates of the points constituting the simulation result meshes while retaining the original connectivity between points. The meshes, with the points arranged as an unstructured grid, were resampled to a rectilinear grid. This was done using Gaussian kernel resampling using the four closest points for interpolation. The result of this operation is a niftii image file for each simulation result containing the norm of the EF at each voxel in the template resolution.

2.4.2. Data reduction

Electric field results were stacked as a 4D matrix to compute 3D stimulation maps. To minimize memory requirements, this was done in sub-regions corresponding to the explored volume in each hemisphere. Different 3D maps were produced, using the simulation results in binary form after excluding voxels with EF norm under 0.2V/mm. This threshold corresponds to the activation of neurons with axon diameters starting from 3 µm–4 µm, at a 60 µs stimulation pulse width (Åström et

al. 2015). The count of EF above the threshold and the number of patients stimulated in each voxel was used to respectively produce the nMap and nPatMap.

In the weighted mean map (wMeanMap), the electric field norm for each stimulation was combined with the symptomatic response in each voxel: the average of the improvement weighted by the electric field norm divided by the stimulation amplitude was computed (Nordin *et al.*, 2022). Voxels in the wMean map with EF norm lower than 0.2V/mm or occurrence scores (nMap) lower than 10% of the max value in the nMap on each side were excluded from the wMeanMap.

2.4.3. Stimulation-effect analysis

To account for variability across patients and provide confidence scores, the EF norm and tremor reduction were linked in a linear mixed model (LMM) for every voxel in space along the stack of simulation results. The model uses tremor improvement as the output variable, EF norm as fixed effect and patient as random effect, with variable slope and intercept for each patient. It allows identifying voxels for which an increase in stimulation strength results in an increase in tremor suppression. The intercepts are kept variable for each patient since we expect different baselines (tremor score without stimulation). The slopes have not been fixed, as they correspond to different response rates for each patient. Moreover, every voxel will be at different locations relative to the active contact in each patient and each test.

A signed p-map was constructed using the sign of the slope (positive or negative response to an increase in stimulation) and the p-value of this slope. Only voxels with $||p|| < 0.05$ were kept and used to mask the wMeanMap. This resulted in two maps, presenting respectively voxels significant for positive and negative relationships (wMeanMap_pPos, wMeanMap_pNeg). The process of creating the probabilistic stimulation-effect map is illustrated in Figure 3.

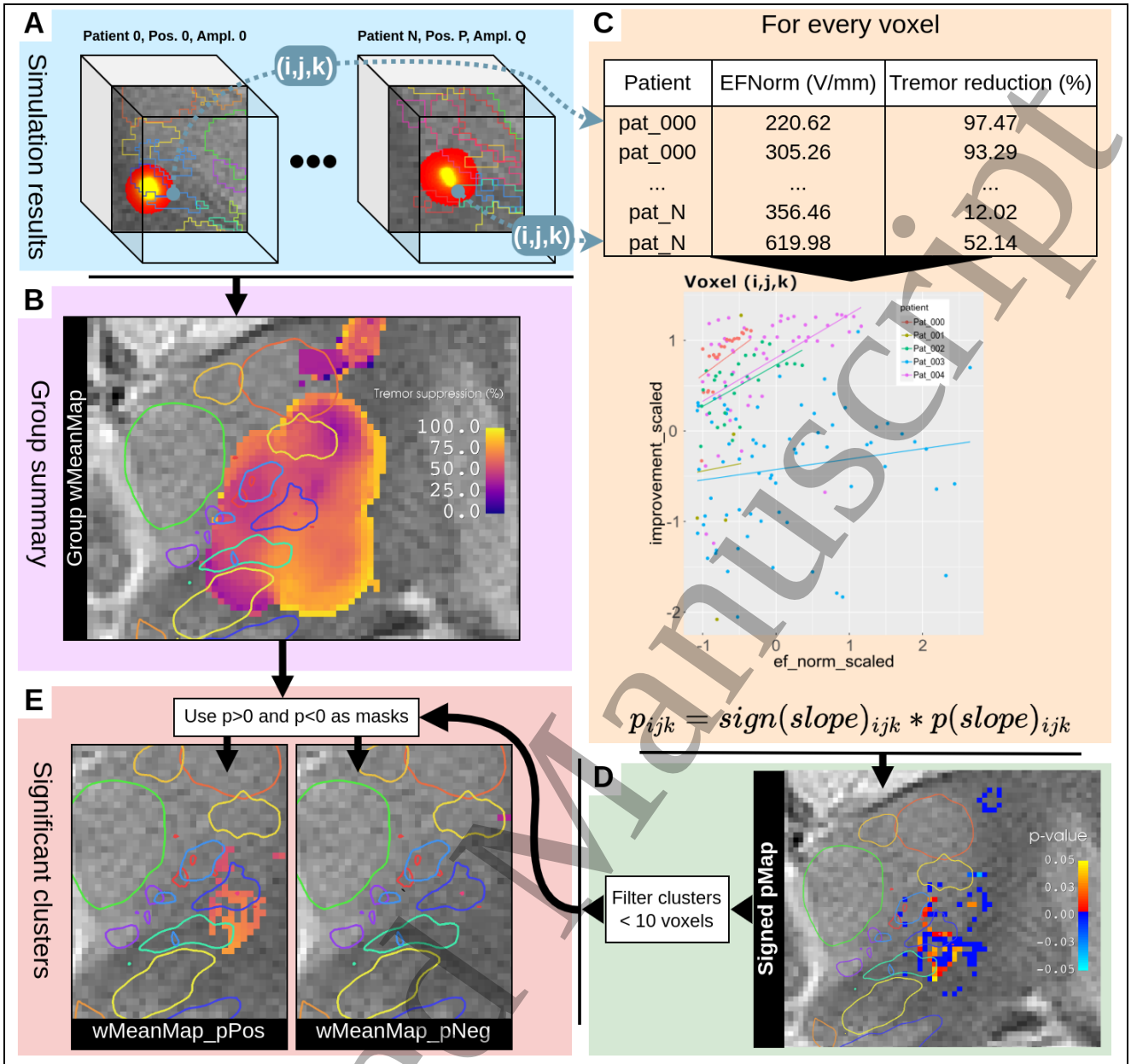

Figure 3: Summarizing overlapping stimulation results for each voxel. The result of each simulation is the norm of the electric field (EF) in each voxel for each combination of stimulation conditions (A). A group-level average effect map is generated (B). To estimate significance in each voxel, the norm of EF and the tremor reduction in all patients are used in a linear mixed model with the patient as grouping variable to estimate the linear relationship between the two variables (C). The confidence level provided for the slope and the sign of that slope is used to build a signed p-map (D). The significant (p<0.05) positive and negative regions are used to mask the wMeanMap (E).

2.5. Verification

The scores predicted by the positive and negative significant maps were compared to the clinical scores obtained for each stimulation test. Each EF was binarized with a 0.2V/mm threshold to create volume of tissue activated (VTA). For each of these, the scores of the voxels from the significant clusters included in the VTA were averaged to obtain a predicted score. Only clusters with more than

10 voxels were considered in this analysis. The correlation between the predicted and measured scores for each cluster was then obtained with Pearson's correlation coefficient.

The clusters obtained in the left brain were compared to the significant cluster obtained by Nowacki and colleagues (Nowacki *et al.*, 2022). In their study, Nowacki and colleagues analyzed the long-term stimulation-effect for 119 patients implanted in Vim/PSA and obtained a significant cluster using Wilcoxon signed ranked test after subdividing the cohort into three equal groups with suboptimal, good and excellent improvement. Their data was obtained from the Lead-DBS data archive available at lead-dbs.org (Treu *et al.*, 2020). The PSM of the intraoperative data was transformed from the group-specific template T1 image to the T1 MNI2009b template using ANTS-SyN. Absolute volumes for each cluster, the distances between their centers of mass, as well as the Dice coefficient describing the overlap between our clusters and the one from Nowacki and colleagues were computed.

2.6. Computing resources

All the steps in the creation of the stimulation maps (anatomical normalization, EF simulations, EF post-processing, data reduction, and analysis) were run on a 32-core AMD 2990WX 3.80 GHz workstation equipped with 128 GB of RAM. Image processing tools and EF simulation tools were set up in two Apptainer containers (apptainer.org). The image processing container was generated with NeuroDocker (github.com/kaczmarj/neurodocker).

3. Results

3.1. Probabilistic stimulation maps

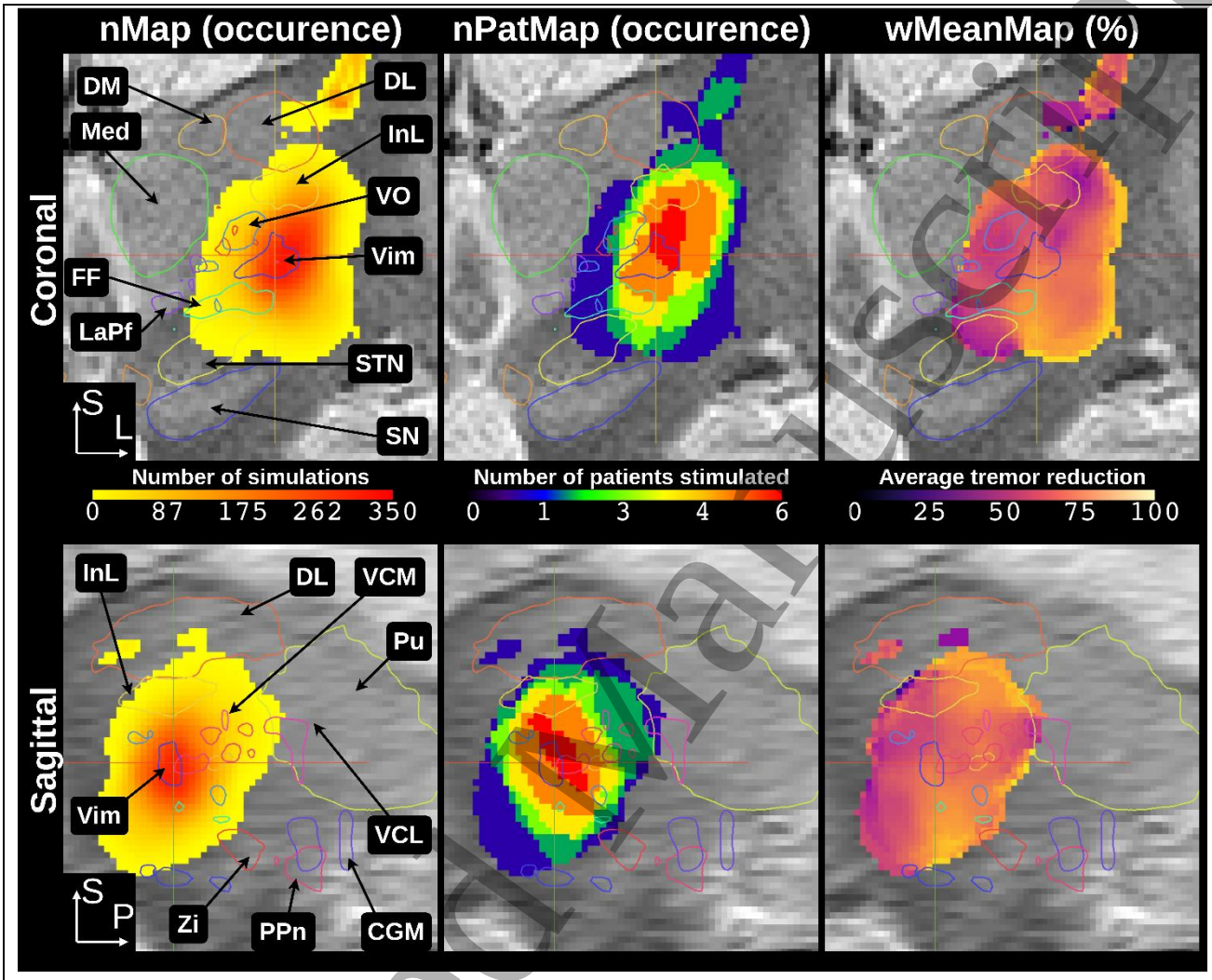

Figure 4: Coronal and sagittal slices in the left hemisphere of the different descriptive statistics maps generated in template space. The nMap (1st column) presents the number of stimulation tests that occurred in each voxel, independent of the patient. Slices were taken at the maximal intensity of the nMap (n=349). The nPatMap (2nd column) presents the number of patients that were stimulated in each voxel. The wMeanMap (3rd column) presents the average tremor reduction observed in each voxel.

Group-level data is presented in Figure 4. The nMap presents the number of stimulation tests in all patients that occurred in each voxel, with a maximum of 349. The distribution shows an oval tendency centered on Vim. The nPatMap presents the number of patients that have been stimulated at least once in each voxel. In this case, the distribution is similar but shifted superior and posterior to Vim. Finally, the wMeanMap presents the average tremor reduction among all patients for each voxel. The voxels with the highest improvement scores, including data from several patients, concentrate in the region inferior-posterior to Vim at the lateral border of the Field of Forel (FF) and STN. The region responsible for the lowest improvement is superior-anterior to Vim, i.e. at the positions before

the target during the exploration. Voxels at the border of the explored region show very contrasting scores because of the few samples included.

The pMap for the slopes in the LMM is presented in Figure 5. The slices presented are taken at the same location as Figure 4 for method illustration purposes. Very few voxels present a significant negative relationship between tremor reduction and EF norm (violet voxels, white arrow). They concentrate in the early region of the exploration in the lateral third of the intermediolateral thalamus (InL).

Figure 6 presents the same data at slices intersecting the clusters significative for improvement, located in the region inferior to Vim and at the limit between Vim and the ventro-oral nucleus (VO) and ventro-caudal nucleus (VC). The first cluster is denoted “PSA cluster” (Posterior subthalamic area) corresponding to the region including FF, the prelemniscal radiations (PLR) and zona incerta (Zi); the second one “Vim-VO cluster.”

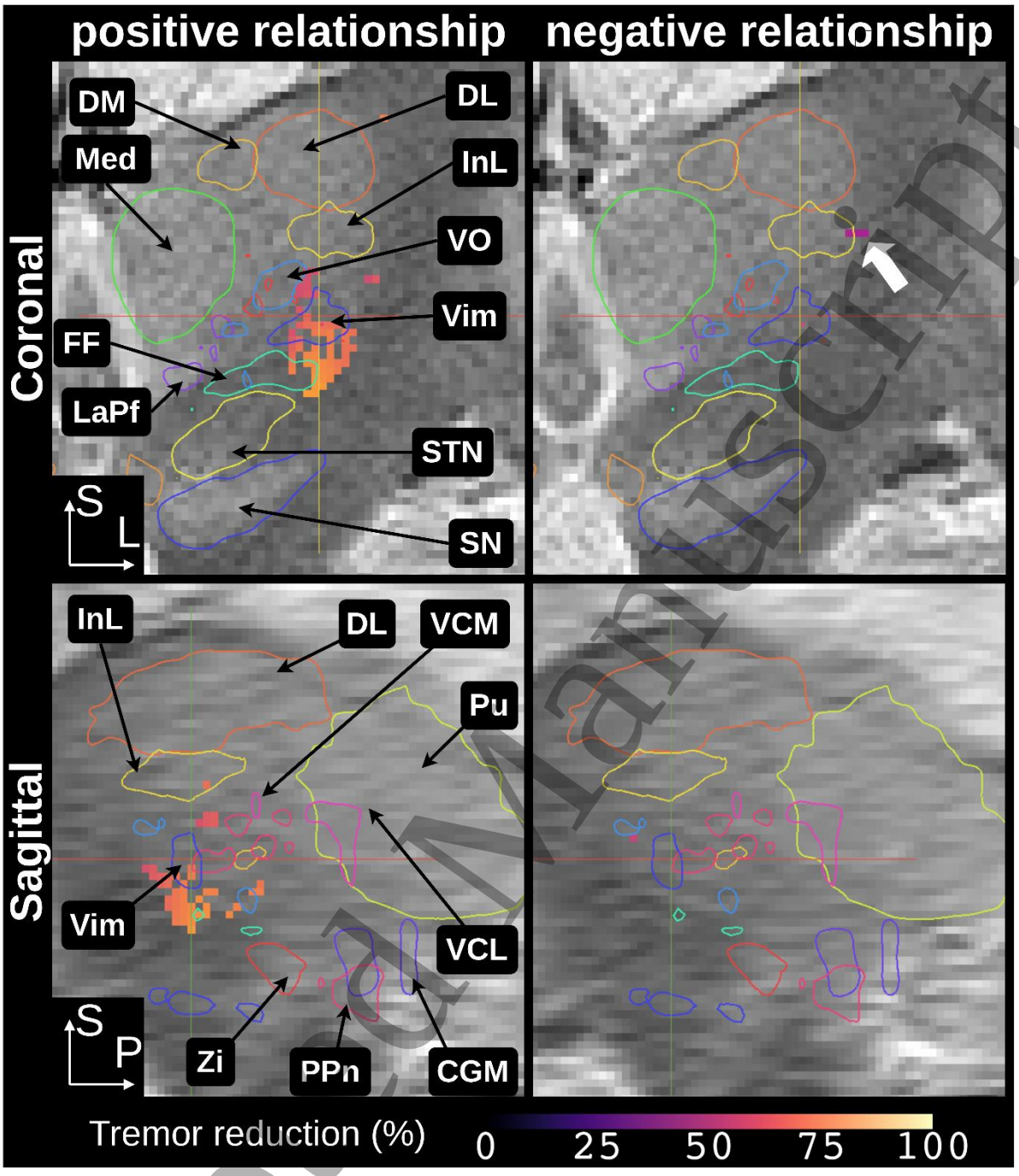

Figure 5: Coronal and sagittal slices in the left hemisphere taken at the same location as Figure 4. On the left and right side respectively, the voxels from the wMeanMap provided a significantly positive and negative (white arrow) relationship between electric field norm and tremor reduction.

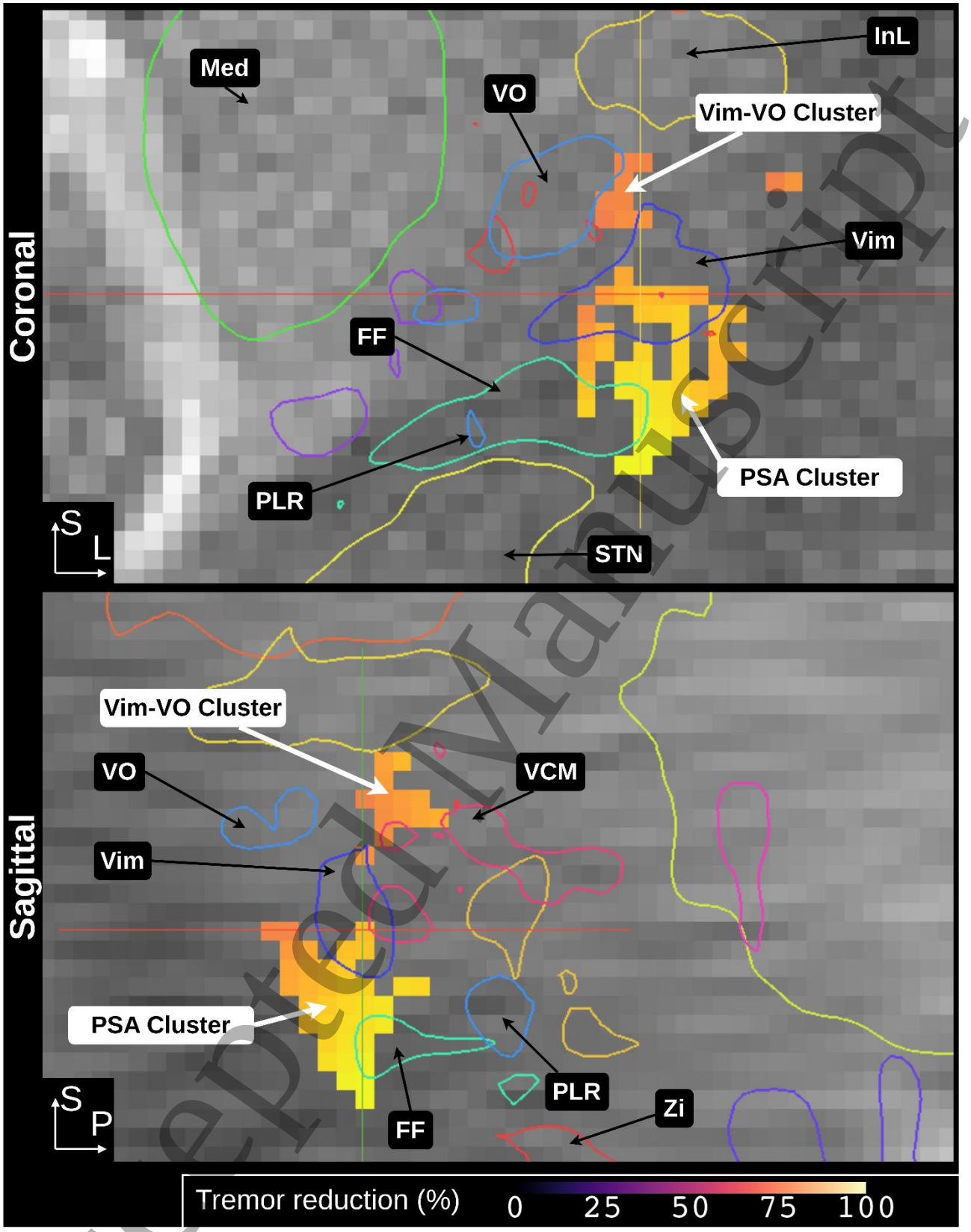

Figure 6: Coronal and Sagittal slices in the left hemisphere of the PSM significant for positive correlation between the electric field norm and tremor reduction. The slice location was selected to present both PSA and Vim-VO clusters.

3.2. Verification

The average of the improvement values in the intersection between each EF and wMeanMap clusters are presented in Figure 7 against the tremor reduction score measured during surgery. Linear correlation and distributions of each variable are provided. The largest clusters are located at the limit between Vim and VO and in the PSA. On the left side only, a cluster is also present anterior and superior to Vim (i.e. before Vim along exploration trajectories). The correlation is significant for both Vim-VO and PSA clusters on both sides but not for the superior-anterior cluster on the left side. For the Vim-VO and PSA clusters, results are complementary between sides: on the left side the PSA cluster has the most samples, lower R-value (Left: PSA: 0.25, Vim-VO: 0.31) and higher mean intersection score values (inter_mean) scores than the Vim-VO cluster while on the right side, the Vim-VO cluster has those characteristics when compared to the right PSA cluster (Right: Vim-VO: 0.27, PSA: 0.49). The distribution of clinical improvement scores (density plots, top) indicates a higher concentration of tremor reduction scores towards high values (80-100%) on the right side than on the left.

Figure 8 presents the visual comparison between the significant cluster obtained by Nowacki et al. (Nowacki et al., 2022) and the Vim-VO and PSA clusters presented in this study. The cluster from Nowacki is more spheric than the two clusters obtained in this study and has a volume of 484mm^3. The clusters in this study have a volume of 118.5mm^3 and 54mm^3 for the Vim-Vo and the PSA cluster respectively. The Vim-VO cluster of this study does not have any contact with the cluster from Nowacki, while the PSA cluster has a Dice coefficient of 0.4 with the cluster from Nowacki. The Vim-VO cluster has its center 4.32mm left, 3.43mm anterior and 18.95mm superior to the one from Nowacki, while the center of the PSA cluster is 0.94mm left, 2.10mm anterior and 4.21mm superior to it.

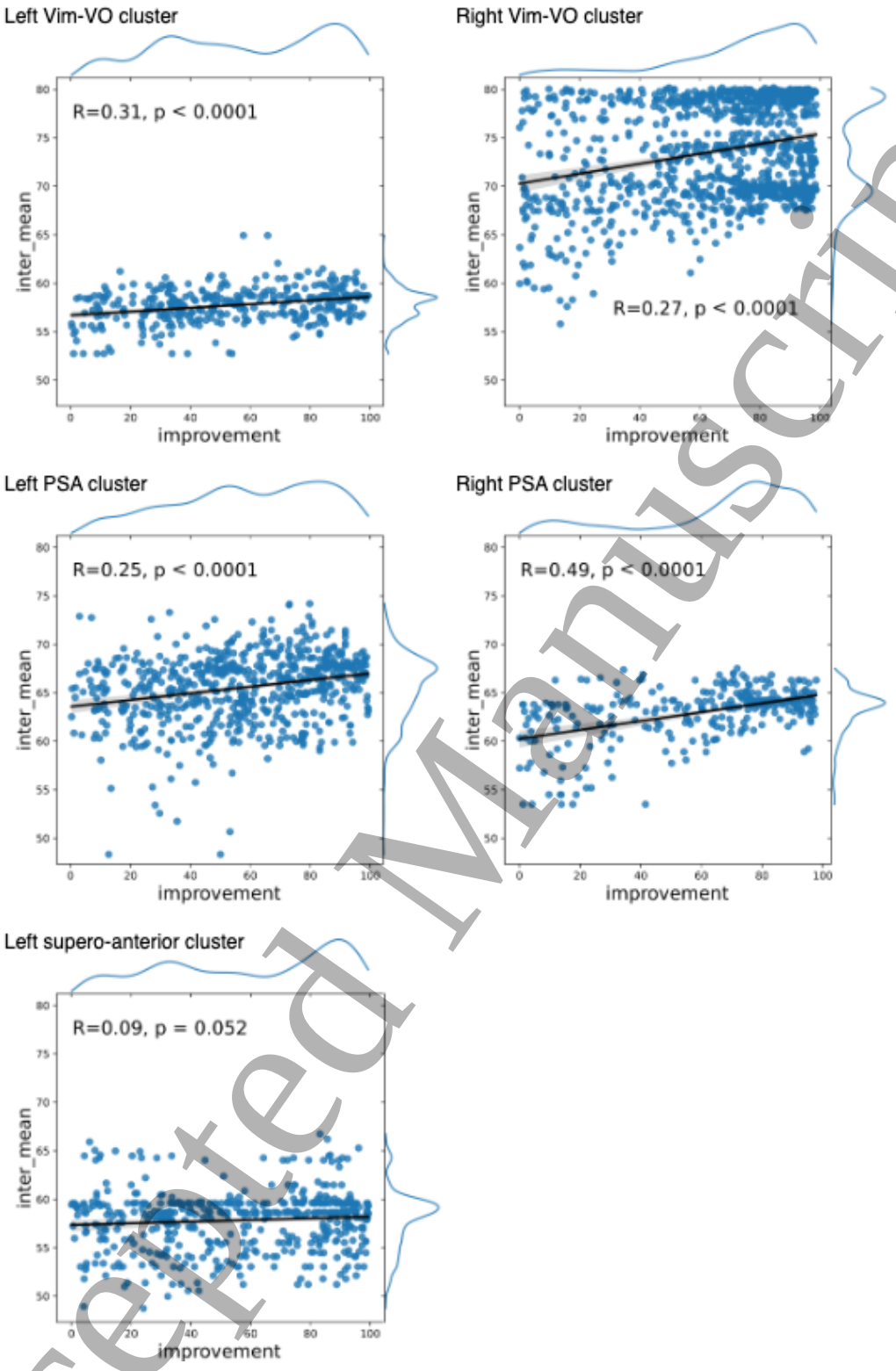

Figure 7: PSM verification. Linear correlation between predicted (inter_mean, y-axis) and measured tremor reduction score (improvement, x-axis). The predicted score is the average score in the intersection volume between each cluster in the PSM and the binary form of each of the original VTAs (volume of tissue activated, n=1821) used for generating the PSM. Columns: Brain hemisphere (left/right), rows: cluster (PSA/Vim-VO/superior-anterior cluster)

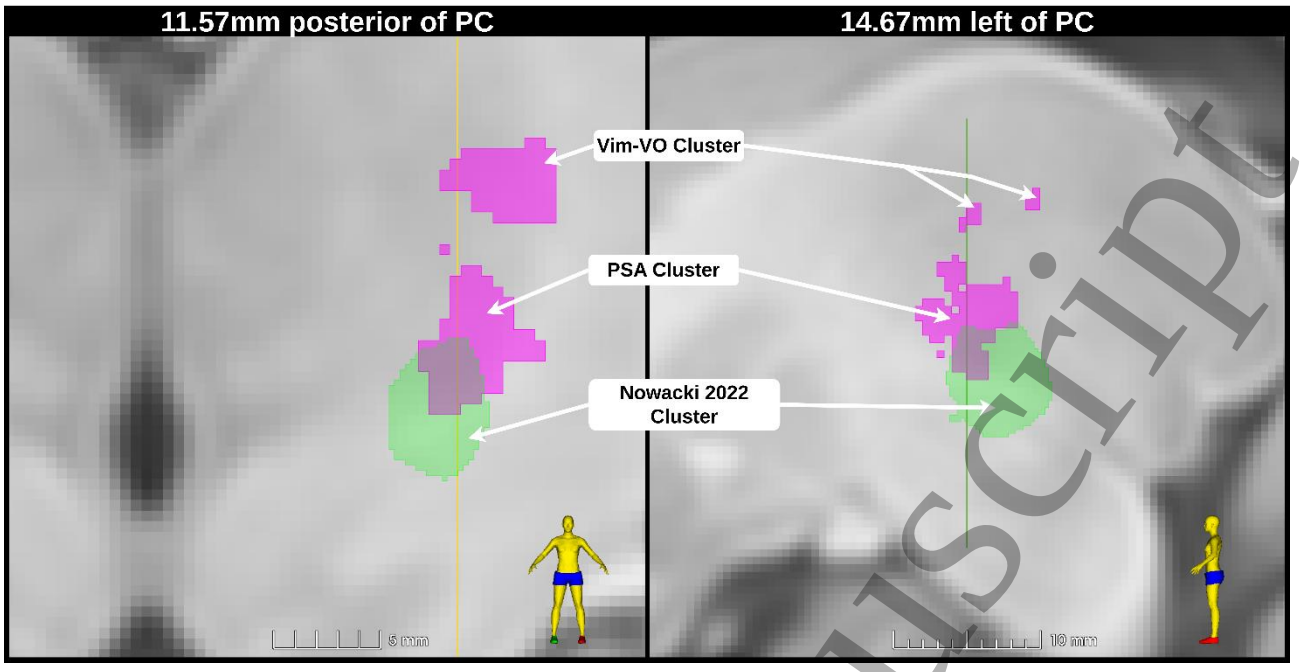

Figure 8: Comparison with results from (Nowacki et al.*, 2022) on the left hemisphere in MNI space. Coronal (left) and sagittal (right) slices of the significant clusters, in purple the two main clusters identified in this study (PSA cluster and Vim-VO cluster) and in green the cluster from Nowacki and colleagues.*

4. Discussion

The primary goal of this paper was to develop and implement a workflow specially tailored for the exploration of probabilistic stimulation mapping derived from intra-operative test stimulation data in the Vim for ET patients. It combines a group-specific, asymmetric normalization procedure, patient-specific EF simulations, and quantitative tremor assessment. Through its application to six ET patients, we were able to pinpoint regions in the PSA and at the boundary between Vim and VO-Vc which provided a positive response to stimulation.

4.1. Probabilistic maps

In the present paper, we applied three analysis methods, i.e. the nMap, nPatMap and wMeanMap, which have previously been presented in the literature for probabilistic mapping of Vim for ET (Dembek *et al.*, 2017; Nowacki *et al.*, 2022), STN for PD (Akram *et al.*, 2017; Dembek *et al.*, 2019; Nguyen *et al.*, 2019) and Globus Pallidus Internus (GPi) for Tourette Syndrome (Akbarian-Tefaghi *et al.*, 2017; Johnson *et al.*, 2019). Unlike most of the previous studies which used data from contact evaluation weeks or months after surgery, together with generic symmetric brain templates, we evaluated intra-operative test data using an in-house generated asymmetric group-specific template. The latter captured differences in response between sides. The wMeanMap presents an overview of the stimulation response but does not transcribe any kind of statistical significance. As a result, most of the highest improvement voxels lie in the periphery of the map where only a few samples

are present. It is useful as a summary of the data but not for interpretation. In consequence, voxels are generally classified and clustered using statistical methods such as Wilcoxon (Dembek *et al.*, 2017; Nguyen *et al.*, 2019) or t-test (Frankemolle *et al.*, 2010; Eisenstein *et al.*, 2014; Nordin *et al.*, 2022). A few previous studies used LMM to classify contact locations (Dafsari *et al.*, 2018) or for verification (Dembek *et al.*, 2019). The choice of the voxel-wise LMM in the present study was motivated by the very unbalanced nature of the dataset, with few patients, but many samples (stimulation tests) per patient. Therefore, using a t-test against a fixed improvement as proposed by Eisenstein et al. was not sufficient (Eisenstein *et al.*, 2014). Despite the small number of patients, LMM reached significance in the inferior part of the cluster, where a total of 86 stimulation tests in four out of six patients were present, while most of the voxels with very high number of samples were deemed non-significant.

We used the sign of the slope estimated by the LMM to classify voxels contribution. Voxels were considered net positive contributors when an increase in stimulation strength resulted in a significant decrease in tremor and inversely for negative voxels. This has the advantage of considering the relationship between the strength of the stimulation and tremor reduction, unlike the t-test which compares the scores in the wMeanMap in absolute values.

The anatomical location of the two clusters presented in Figure 6 are in the PSA region, which is a common target for ET-DBS, and in the Vim-VO junction proposed more recently (Pouratian *et al.*, 2011; Elias *et al.*, 2021; Middlebrooks *et al.*, 2021). These seem to be both alternative afferent points for influencing the dentato-rubro-thalamic tract (DRTT). In our previous study, we generated patient-specific stimulation maps for each of the patients used in this study and analyzed the overlap with anatomical structures and he importance of the PSA and VO/Vc was also prominent (Shah *et al.*, 2015, 2020).

4.2. Verification

The PSM clusters were compared against the original EF with the mean intersection score. Linear correlation was used to compare PSM clusters against the clinical score. Data from the PSA and Vim-VO clusters were deemed significant. Distribution of the samples, R, and p-values of the linear correlation show an alternating pattern between hemispheres. Similar verification methods were applied in previous studies (Elias *et al.*, 2021; Neudorfer *et al.*, 2023). Elias et al., presented R-values of 0.65 and Neudorfer and colleagues between 0.32 and 0.48. The results in this study are in the same range, despite the inclusion of all intra-operative stimulation tests which results in a larger variance in the input data compared to studies considering only those with the highest improvement for each contact. With these R-values, the corresponding R^2 values are below 0.5, thus the linear correlation model describes less than 50% of the variance in predicted reduction. Unlike the two aforementioned studies, the verification in our study used the same data as for the creation of the PSM. While patient leave-one-out cross-validation would have been superior, the low number of

patients makes it un-practical since removing an entire patient results in a massive change in the dataset. In consequence, the verification does not represent a clinical validation of the map, proving any kind of universality to predict outcomes in new patients. Instead, it ascertains that the workflow did not diverge from the original clinical data.

When comparing the PSA cluster with results from Nowacki and colleagues on long term ET data, a distance of less than 5mm between the center of the clusters was observed. This difference could partially be caused by different methodological approaches such as image fusion (only based on T1, so low contrast for Vim) or the PSM generation (linear mixed model versus Wilcoxon ranked test). The main difference is certainly the kind of available data . Even with the low number of patients, the results obtained from intra-operative stimulation test data are encouraging. The application of this method to more patients with high resolution data might be able to refine these clusters.

The use of an asymmetric anatomical reference and the separate analysis of each side revealed the lateralized response of the clusters. A potential reason for the asymmetry may be the brain shift expected on the second side in bilateral implantations. This was not considered in the workflow. This is however contradicted by the better improvements on the second implantation side. Another possibility is the inherent difference in response to stimulation from each side. Bilateral implantations being associated with more occurrence of gait and speech deficits than unilateral in ET-Vim-DBS (Mitchell *et al.*, 2019; Kim *et al.*, 2021; Prakash *et al.*, 2022). Probabilistic mapping of the occurrence of adverse events could confirm it, but this dataset is too small and further studies are required.

4.3. Intra-operative vs post-operative stimulation

To the best of our knowledge, the present study is the first example of a probabilistic study making use of data collected intra-operatively in contrast with the rest of the literature using post-operative/chronic/long-term stimulation settings and effects. Despite being a common approach to identify the best location for implantation, the ability of intra-operative tests to predict post-operative stimulation settings has been questioned (Lafreniere-Roula *et al.*, 2009; Geraedts *et al.*, 2019). In this study, we show that thanks to the richness of the data collected during intra-operative stimulation tests, the probabilistic mapping can provide results that agree with those from studies using data from chronic stimulation despite few subjects being included.

4.4. Limitations and future possibilities

The main limitation of the study is the low number of patients included limiting the potential to generalize conclusions to new patients. Even if the high number of fields included for each individual resulted in statistical significance and to isolate sweet spot clusters in the PSM, the low number of patients limits the transferability. More patients are planned to be included in the next step, opening the door to leave-one-out or out-of-cohort validation and thus more reliable conclusions on the prediction capacity of the identified sweet spots. Using a dataset sourced from another center is

difficult at this point, as no dataset to our knowledge is comparable to this one. Especially, using screening or chronic data for validation would test the deviation between intra-operative and chronic stimulation rather than between the PSM and the new patients.

This study did not include any analysis of stimulation-induced adverse effects, which may add crucial information with the identification of regions to avoid. The reason is the low occurrence of those in the dataset, thus their analysis would not have been representative.

Lastly, the anatomical template used as a reference here is specific to the groups to guarantee optimal group data analysis. After the integration of more patients to increase the statistical confidence, the template will be registered to MNI space for the comparison of the presented results with those from other studies.

5. Conclusion

In this study, we implemented a workflow and demonstrated the potential for the creation of probabilistic stimulation maps from data generated during intra-operative stimulation tests. With more stimulation amplitudes and positions tested and a larger anatomical volume explored than in chronic situations, promising results were obtained from six patients. The region posterior to Vim and lateral to the FF (PSA) as well as the border between Vim and VO were identified to positively respond to stimulation, corroborating chronic DBS studies. This work underlines the potential of data collected intra-operatively as a source of high-resolution data for precisely pinpointing the DBS “sweet spot” for essential tremor.

Acknowledgments

This work was supported by the University of Applied Sciences and Arts Northwestern Switzerland, the Swedish foundation for strategic research [grant number BD15-0032],the Swedish Research Council [grant number 2016-03564] and the Swiss National Science Foundation [205320_207491].

Conflict of interest: None

Author contributions:

Dorian Vogel: Conceptualization; Methodology; Software; Validation; Formal analysis; Investigation; Data Curation; Writing – original draft preparation; Writing – review and editing; Visualization.

Teresa Nordin: Conceptualization; Methodology; Writing – review and editing.

Stefanie Feiler: Methodology (Statistics); Writing – review and editing.

Karin Wårdell: Conceptualization; Writing – original draft preparation; Writing – review and editing; Supervision; Project administration; Funding acquisition.

Jérôme Coste: Validation; Investigation; Resources; Data Curation; Writing – review and editing.

Jean-Jacques Lemaire: Validation; Investigation; Resources; Data Curation; Writing – review and editing.

Simone Hemm: Conceptualization; Methodology; Writing – original draft preparation; Writing – review and editing; Visualization; Supervision; Project administration; Funding acquisition.

References

Akbarian-Tefaghi, L. *et al.* (2017) 'Refining the Deep Brain Stimulation Target within the Limbic Globus Pallidus Internus for Tourette Syndrome', *Stereotactic and Functional Neurosurgery*, 95(4), pp. 251–258. Available at: https://doi.org/10.1159/000478273.

Akram, H. *et al.* (2017) 'Subthalamic deep brain stimulation sweet spots and hyperdirect cortical connectivity in Parkinson's disease', *NeuroImage*, 158, pp. 332–345. Available at: https://doi.org/10.1016/j.neuroimage.2017.07.012.

Akram, H. *et al.* (2018) 'Connectivity derived thalamic segmentation in deep brain stimulation for tremor', *NeuroImage: Clinical*, 18, pp. 130–142. Available at: https://doi.org/10.1016/j.nicl.2018.01.008.

Aström, M. *et al.* (2009) 'Method for patient-specific finite element modeling and simulation of deep brain stimulation', *Medical & Biological Engineering & Computing*, 47(1), pp. 21–28. Available at: https://doi.org/10.1007/s11517-008-0411-2.

Åström, M. *et al.* (2009) 'Method for patient-specific finite element modeling and simulation of deep brain stimulation', *Medical & Biological Engineering & Computing*, 47(1), pp. 21–28. Available at: https://doi.org/10.1007/s11517-008-0411-2.

Åström, M. *et al.* (2015) 'Relationship between Neural Activation and Electric Field Distribution during Deep Brain Stimulation', *IEEE Transactions on Biomedical Engineering*, 62(2), pp. 664–672. Available at: https://doi.org/10.1109/TBME.2014.2363494.

Åström, M. *et al.* (2018) 'Prediction of Electrode Contacts for Clinically Effective Deep Brain Stimulation in Essential Tremor', *Stereotactic and Functional Neurosurgery*, 96(5), pp. 281–288. Available at: https://doi.org/10.1159/000492230.

Åström, M., Lemaire, J.-J. and Wårdell, K. (2012) 'Influence of heterogeneous and anisotropic tissue conductivity on electric field distribution in deep brain stimulation', *Medical & Biological Engineering & Computing*, 50(1), pp. 23–32. Available at: https://doi.org/10.1007/s11517-011-0842-z.

Avants, B.B. *et al.* (2010) 'Ants: Open-source tools for normalization and neuroanatomy'.

Barbe, M.T. *et al.* (2018) 'DBS of the PSA and the VIM in essential tremor: A randomized, double-blind, crossover trial', *Neurology*, 91(6), pp. e543–e550. Available at: https://doi.org/10.1212/WNL.0000000000005956.

Benabid, A.L. *et al.* (1993) 'Chronic VIM thalamic stimulation in Parkinson's disease, essential tremor and extra-pyramidal dyskinesias', *Acta Neurochir Suppl (Wien)*, 58, pp. 39–44.

Benabid, A.L. *et al.* (1994) 'Acute and Long-Term Effects of Subthalamic Nucleus Stimulation in Parkinson's Disease', *Stereotactic and Functional Neurosurgery*, 62(1–4), pp. 76–84. Available at: https://doi.org/10.1159/000098600.

Beninca, J. *et al.* (2017) 'Software for Stereotactic Surgery Planning', *Neurotarget*, 11(N˚4 2017), p. 37.

Butenko, K. *et al.* (2020) 'OSS-DBS: Open-source simulation platform for deep brain stimulation with a comprehensive automated modeling', *PLOS Computational Biology*. Edited by D. Marinazzo, 16(7), p. e1008023. Available at: https://doi.org/10.1371/journal.pcbi.1008023.

Butson, C.R. *et al.* (2007) 'Patient-specific analysis of the volume of tissue activated during deep brain stimulation', *NeuroImage*, 34(2), pp. 661–670. Available at: https://doi.org/10.1016/j.neuroimage.2006.09.034.

Dafsari, H.S. *et al.* (2018) 'Non-motor outcomes of subthalamic stimulation in Parkinson's disease depend on location of active contacts', *Brain Stimulation*, 11(4), pp. 904–912. Available at: https://doi.org/10.1016/j.brs.2018.03.009.

Dembek, T.A. *et al.* (2017) 'Probabilistic mapping of deep brain stimulation effects in essential tremor', *NeuroImage: Clinical*, 13, pp. 164–173. Available at: https://doi.org/10.1016/j.nicl.2016.11.019.

Dembek, T.A. *et al.* (2019) 'Probabilistic sweet spots predict motor outcome for deep brain stimulation in Parkinson disease', *Annals of Neurology*, 86(4), pp. 527–538. Available at: https://doi.org/10.1002/ana.25567.

Eisenstein, S.A. *et al.* (2014) 'Functional anatomy of subthalamic nucleus stimulation in Parkinson disease: STN DBS Location and PD', *Annals of Neurology*, 76(2), pp. 279–295. Available at: https://doi.org/10.1002/ana.24204.

Elias, G.J.B. *et al.* (2021) 'Probabilistic Mapping of Deep Brain Stimulation: Insights from 15 Years of Therapy', *Annals of Neurology*, 89(3), pp. 426–443. Available at: https://doi.org/10.1002/ana.25975.

Ewert, S. *et al.* (2019) 'Optimization and comparative evaluation of nonlinear deformation algorithms for atlas-based segmentation of DBS target nuclei', *NeuroImage*, 184, pp. 586–598. Available at: https://doi.org/10.1016/j.neuroimage.2018.09.061.

Fedorov, A. *et al.* (2012) '3D Slicer as an image computing platform for the Quantitative Imaging Network', *Magnetic Resonance Imaging*, 30(9), pp. 1323–1341. Available at: https://doi.org/10.1016/j.mri.2012.05.001.

Fonov, V. *et al.* (2009) 'Unbiased nonlinear average age-appropriate brain templates from birth to adulthood', *NeuroImage*, 47, p. S102. Available at: https://doi.org/10.1016/S1053-8119(09)70884-5.

Frankemolle, A.M.M. *et al.* (2010) 'Reversing cognitive–motor impairments in Parkinson's disease patients using a computational modelling approach to deep brain stimulation programming', *Brain*, 133(3), pp. 746–761. Available at: https://doi.org/10.1093/brain/awp315.

Gabriel, S., Lau, R.W. and Gabriel, C. (1996) 'The dielectric properties of biological tissues: III. Parametric models for the dielectric spectrum of tissues', *Physics in Medicine and Biology*, 41(11), pp. 2271–2293. Available at: https://doi.org/10.1088/0031-9155/41/11/003.

Geraedts, V.J. *et al.* (2019) 'Intraoperative test stimulation of the subthalamic nucleus aids postoperative programming of chronic stimulation settings in Parkinson's disease', *Parkinsonism & Related Disorders*, 65, pp. 62–66. Available at: https://doi.org/10.1016/j.parkreldis.2019.05.017.

Hariz, M. (2017) 'My 25 Stimulating Years with DBS in Parkinson's Disease', *Journal of Parkinson's Disease*, 7(s1), pp. S33–S41. Available at: https://doi.org/10.3233/JPD-179007.

Horn, A. *et al.* (2019) 'Lead-DBS v2: Towards a comprehensive pipeline for deep brain stimulation imaging', *NeuroImage*, 184, pp. 293–316. Available at: https://doi.org/10.1016/j.neuroimage.2018.08.068.

Horn, A. and Blankenburg, F. (2016) 'Toward a standardized structural–functional group connectome in MNI space', *NeuroImage*, 124, pp. 310–322. Available at: https://doi.org/10.1016/j.neuroimage.2015.08.048.

Howell, B. and McIntyre, C.C. (2017) 'Role of Soft-Tissue Heterogeneity in Computational Models of Deep Brain Stimulation', *Brain Stimulation*, 10(1), pp. 46–50. Available at: https://doi.org/10.1016/j.brs.2016.09.001.

Johansson, J.D., Alonso, F. and Wårdell, K. (2019) 'Patient-Specific Simulations of Deep Brain Stimulation Electric Field with Aid of In-house Software ELMA', in *2019 41st Annual International Conference of the IEEE Engineering in Medicine and Biology Society (EMBC)*. *2019 41st Annual International Conference of the IEEE Engineering in Medicine and Biology Society (EMBC)*, pp. 5212–5216. Available at: https://doi.org/10.1109/EMBC.2019.8856307.

Johnson, K.A. *et al.* (2019) 'Image-based analysis and long-term clinical outcomes of deep brain stimulation for Tourette syndrome: a multisite study', *Journal of Neurology, Neurosurgery & Psychiatry*, 90(10), pp. 1078–1090. Available at: https://doi.org/10.1136/jnnp-2019-320379.

Kim, M.J. *et al.* (2021) 'Stimulation-Induced Side Effects of Deep Brain Stimulation in the Ventralis Intermedius and Posterior Subthalamic Area for Essential Tremor', *Frontiers in Neurology*, 12. Available at: https://www.frontiersin.org/article/10.3389/fneur.2021.678592 (Accessed: 18 April 2022).

Lafreniere-Roula, M. *et al.* (2009) 'Microstimulation-induced inhibition as a tool to aid targeting the ventral border of the subthalamic nucleus: Clinical article', *Journal of Neurosurgery*, 111(4), pp. 724–728. Available at: https://doi.org/10.3171/2009.3.JNS09111.

Lalys, F. *et al.* (2013) 'Anatomo-clinical atlases correlate clinical data and electrode contact coordinates: Application to subthalamic deep brain stimulation', *Journal of neuroscience methods*, 212(2), pp. 297–307.

Lemaire, J.-J. *et al.* (2010) 'Anatomy of the Human Thalamus Based on Spontaneous Contrast and Microscopic Voxels in High-Field Magnetic Resonance Imaging':, *Operative Neurosurgery*, 66, pp. ons161–ons172. Available at: https://doi.org/10.1227/01.NEU.0000365617.41061.A3.

Lemaire, J.-J. *et al.* (2019) 'MRI Atlas of the Human Deep Brain', *Frontiers in Neurology*, 10, p. 851. Available at: https://doi.org/10.3389/fneur.2019.00851.

Lemaire, J.-J. (2021) *Textbook on MRI Mapping of the Human Deep Brain: Maps and Extended 3D Analysis*, *Textbook on MRI Mapping of the Human Deep Brain*. EDP Sciences. Available at: https://doi.org/10.1051/978-2-7598-2576-9.

Lozano, A.M. *et al.* (2019) 'Deep brain stimulation: current challenges and future directions', *Nature Reviews Neurology*. Available at: https://doi.org/10.1038/s41582-018-0128-2.

Magnotta, V.A. *et al.* (2000) 'Visualization of Subthalamic Nuclei with Cortex Attenuated Inversion Recovery MR Imaging', *NeuroImage*, 11(4), pp. 341–346. Available at: https://doi.org/10.1006/nimg.2000.0552.

Middlebrooks, E.H. *et al.* (2021) 'Connectivity correlates to predict essential tremor deep brain stimulation outcome: Evidence for a common treatment pathway', *NeuroImage: Clinical*, 32, p. 102846. Available at: https://doi.org/10.1016/j.nicl.2021.102846.

Mitchell, K.T. *et al.* (2019) 'Benefits and risks of unilateral and bilateral ventral intermediate nucleus deep brain stimulation for axial essential tremor symptoms', *Parkinsonism & Related Disorders*, 60, pp. 126–132. Available at: https://doi.org/10.1016/j.parkreldis.2018.09.004.

Morel, A. (2007) *Stereotactic Atlas of the Human Thalamus and Basal Ganglia*. 0 edn. CRC Press. Available at: https://doi.org/10.3109/9781420016796.

Neudorfer, C. *et al.* (2023) 'Lead-DBS v3.0: Mapping deep brain stimulation effects to local anatomy and global networks', *NeuroImage*, 268, p. 119862. Available at: https://doi.org/10.1016/j.neuroimage.2023.119862.

Nguyen, T.A.K. *et al.* (2019) 'Directional stimulation of subthalamic nucleus sweet spot predicts clinical efficacy: Proof of concept', *Brain Stimulation*, 12(5), pp. 1127–1134. Available at: https://doi.org/10.1016/j.brs.2019.05.001.

Nordin, T. *et al.* (2019) 'White matter tracing combined with electric field simulation – A patient-specific approach for deep brain stimulation', *NeuroImage: Clinical*, 24, p. 102026. Available at: https://doi.org/10.1016/j.nicl.2019.102026.

Nordin, T. *et al.* (2022) 'Probabilistic maps for deep brain stimulation – Impact of methodological differences', *Brain Stimulation*, 15(5), pp. 1139–1152. Available at: https://doi.org/10.1016/j.brs.2022.08.010.

Nowacki, A. *et al.* (2022) 'Probabilistic mapping reveals optimal stimulation site in essential tremor', *Annals of Neurology* [Preprint]. Available at: https://doi.org/10.1002/ana.26324.

Nowinski, W.L. *et al.* (2005) 'Statistical Analysis of 168 Bilateral Subthalamic Nucleus Implantations by Means of the Probabilistic Functional Atlas':, *Operative Neurosurgery*, 57, pp. 319–330. Available at: https://doi.org/10.1227/01.NEU.0000180960.75347.11.

Pouratian, N. *et al.* (2011) 'Multi-institutional evaluation of deep brain stimulation targeting using probabilistic connectivity-based thalamic segmentation: Clinical article', *Journal of Neurosurgery*, 115(5), pp. 995–1004. Available at: https://doi.org/10.3171/2011.7.JNS11250.

Prakash, P. *et al.* (2022) 'Benefits and Risks of a STAGED-BILATERAL VIM Versus Unilateral VIM DBS for Essential Tremor', *Movement Disorders Clinical Practice*, 9(6), pp. 775–784. Available at: https://doi.org/10.1002/mdc3.13490.

Roquemaurel, A. de *et al.* (2021) 'Stimulation Sweet Spot in Subthalamic Deep Brain Stimulation – Myth or Reality? A Critical Review of Literature', *Stereotactic and Functional Neurosurgery*, pp. 1–18. Available at: https://doi.org/10.1159/000516098.

Schaltenbrand, G. (1977) 'Atlas for stereotaxy of the human brain', *Georg Thieme* [Preprint].

Shah, A. *et al.* (2015) 'Use of quantitative tremor evaluation to enhance target selection during deep brain stimulation surgery for essential tremor', *Current Directions in Biomedical Engineering*, 1(1). Available at: https://doi.org/10.1515/cdbme-2015-0117.

Shah, A. *et al.* (2017) 'Intraoperative acceleration measurements to quantify improvement in tremor during deep brain stimulation surgery', *Medical & Biological Engineering & Computing*, 55(5), pp. 845–858. Available at: https://doi.org/10.1007/s11517-016-1559-9.

Shah, A. *et al.* (2020) 'Stimulation maps: visualization of results of quantitative intraoperative testing for deep brain stimulation surgery', *Medical & Biological Engineering & Computing*, 58(4), pp. 771–784. Available at: https://doi.org/10.1007/s11517-020-02130-y.

Treu, S. *et al.* (2020) 'Deep Brain Stimulation: Imaging on a group level', *NeuroImage*, p. 117018. Available at: https://doi.org/10.1016/j.neuroimage.2020.117018.

Vassal, F. *et al.* (2012) 'Direct stereotactic targeting of the ventrointermediate nucleus of the thalamus based on anatomic 1.5-T MRI mapping with a white matter attenuated inversion recovery (WAIR) sequence', *Brain Stimulation*, 5(4), pp. 625–633. Available at: https://doi.org/10.1016/j.brs.2011.10.007.

Vogel, D. *et al.* (2020) 'Anatomical Brain Structures Normalization for Deep Brain Stimulation in Movement Disorders', *NeuroImage: Clinical*, p. 102271. Available at: https://doi.org/10.1016/j.nicl.2020.102271.

Vogel, D. (2021) '#26250 - Stereoslicer, A Plugin for 3Dslicer to Handle Data from Stereotactic Surgeries.' *24th Congress of the European Society of Stereotactic and Functional Neurosurgery*, Marseille, France, 8 September. Available at: https://www.karger.com/Article/FullText/520618 (Accessed: 12 January 2022).

Vogel, D. *et al.* (2021) 'Atlas Optimization for Deep Brain Stimulation', in T. Jarm et al. (eds) *8th European Medical and Biological Engineering Conference*. Cham: Springer International Publishing (IFMBE Proceedings), pp. 130–142. Available at: https://doi.org/10.1007/978-3-030-64610-3_16.

Wårdell, K. *et al.* (2013) 'Patient-specific brain modelling for deep brain stimulation simulations', in *Neural Engineering (NER), 2013 6th International IEEE/EMBS Conference on*. IEEE, pp. 148–151. Available at: http://ieeexplore.ieee.org/xpls/abs_all.jsp?arnumber=6695893 (Accessed: 16 November 2016).

Wårdell, K., Diczfalusy, E. and Åström, M. (2011) 'Patient-Specific Modeling and Simulation of Deep Brain Stimulation', in A. Gefen (ed.) *Patient-Specific Modeling in Tomorrow's Medicine*. Berlin, Heidelberg: Springer Berlin Heidelberg (Studies in Mechanobiology, Tissue Engineering and Biomaterials), pp. 357–375. Available at: https://doi.org/10.1007/8415_2011_104.

Yelnik, J. *et al.* (2007) 'A three-dimensional, histological and deformable atlas of the human basal ganglia. I. Atlas construction based on immunohistochemical and MRI data', *NeuroImage*, 34(2), pp. 618–638. Available at: https://doi.org/10.1016/j.neuroimage.2006.09.026.